Electron delocalization in $Au_N X_M$ (X=Sc, Ti, Cr, Fe) clusters: A density functional theory and photofragmentation study

Ewald Janssens, Hiromasa Tanaka,* Sven Neukermans, Roger E. Silverans, and Peter Lievens†
Laboratorium voor Vaste-Stoffysica en Magnetisme, Katholieke Universiteit Leuven, B-3001 Leuven, Belgium
(Received 25 September 2003; published 10 February 2004)

The stability of gold clusters doped with transition metal atoms (Sc, Ti, Cr, Fe) is studied with photofragmentation spectroscopy. The recorded stability patterns depend on the kind and the amount of dopants. While for singly doped clusters phenomenological electronic shell-model interpretations are suitable, limits of this model are encountered for more complex systems containing multiple dopants. Density-functional theory calculations were carried out on singly doped Au_5X^+ systems (X=Au, Sc, Ti, Cr, Fe). The electron delocalization behavior suggested by the qualitative description given in [Neukermans et al., Phys. Rev. Lett. **90**, 033401 (2003)] is supported by the calculated molecular-orbital patterns. Dopant dependent differences in atomization energy, atomic-orbital occupancies and local magnetic moments are addressed. Evidence is presented to show that the number of delocalized electrons not only depends on the kind and amount of constituting atoms but also on the shape of the cluster.

DOI: 10.1103/PhysRevB.69.085402 PACS number(s): 36.40.Qv, 36.40.Cg, 31.15.Ew

I. INTRODUCTION

One of the key properties of metal clusters is the delocalization behavior of the valence electrons of the constituent atoms. In simple metal clusters such as alkaline or coinage metal clusters the atomic valence electrons delocalize over the cluster volume. Quantum confinement leads to an electronic shell structure with corresponding magic numbers. This shell structure is reflected in many size dependent properties of the cluster, such as fragmentation energy, ionization energy, electron affinity, and polarizability. The magic numbers can be reproduced using simple ''structureless'' models for the effective potential neglecting the discrete nature of the nuclear charge distribution; only the general shape of the potential is considered to be important.[1,2]

On the other hand, these models do not suffice to describe size dependent properties of small transition metal clusters. The presence of unfilled *d* shells has important consequences: *d* electrons give rise to more directional bonds and there are many low-lying excited states due to the different possibilities to arrange the electrons in the empty *d* states. Properties such as the stability of the cluster can often be discussed in terms of shells of atoms, relating the number of atoms needed to form a compact symmetric structure to an enhanced stability.[3] If the *d* orbitals retain their atomic character and remain localized, the cluster will be magnetic. However, enhanced *s*-*d* and *d*-*d* hybridization will increase the tendency toward itinerant behavior and decrease the local magnetic moments. Therefore the magnetic moment per atom will decrease (although nonmonotonically) with increasing cluster size, i.e., when clusters have more nearest neighbors.[4,5]

The interplay between isotropic interaction (e.g., gold) and directional bonds (e.g., transition metals) can be examined by studying bimetallic clusters. Transition metal doped gold clusters are interesting from several points of view. Doping noble metal clusters with impurities changes the properties of the cluster significantly.[6–15] By using transition metals a certain amount of *s* electrons is added to the system and the structure will change because of the different size of the dopant. Also electrons stemming from an open *d* shell are added to the cluster. The complex *s*-*d* and *d*-*d* hybridization effects between *s* and *d* electrons of both types of atoms will determine the properties of the mixed cluster. Moreover a local magnetic moment is introduced in a small free-electron system.

Recent studies have shown that the structure of small gold clusters clearly differs from other coinage metal clusters: gold clusters prefer to be planar up to fairly large sizes.[16–18] The reason for the planar shape is related to relativistic effects that cause a shrinking of the size of the *s* orbitals and enhance the *s*-*d* hybridization, leading to a preference for more directional Au-Au bonds.[19] Moreover, nanoscale gold systems have appealing properties as building blocks for nanostructured materials as well as nanocatalytic systems.[20,21]

In previous papers we reported photofragmentation experiments on single transition metal atom doped gold clusters ($Au_N X$, X=Sc, Ti, V, Cr, Mn, Fe, Co, Ni, Zn; N=1–45). The observed stability patterns were discussed on the basis of a simple phenomenological shell model, taking into account the electronic structure of the dopant atom.[14,22] The enhanced abundance for Au_5X^+ (X=Cr, Mn, Fe, Co, Zn) was ascribed to the planarity of these clusters, in combination with six delocalized electrons being a magic number for two-dimensional(2D) systems.[23]

In this paper we describe the extension of the experiments toward multiply doped gold clusters ($Au_N X_M$, X=Sc, Ti, Cr, Fe; N=1–40, M=0–3). The clusters were produced in a dual-target dual-laser vaporization source and their stability was probed in photofragmentation experiments. In multiply doped systems the interplay between delocalized electrons and the more localized open *d* shells becomes more important. The limitations of the phenomenological shell models are encountered for these complex systems. For single doped systems density-functional theory (DFT) calculations were

carried out on Au_5X^+ (X=Au, Sc, Ti, Cr, Fe). The molecular orbitals in this work confirm the electron delocalization behavior suggested in the qualitative description given before.[14] The calculations also allow to study dopant dependent properties such as atomization energy, atomic-orbital occupancies and local magnetic moments. An extensive size dependent DFT study for $Au_NZn^{(0,+)}$ (N = 1–6) clusters is presented elsewhere.[15]

II. PRODUCTION OF TRANSITION METAL DOPED GOLD CLUSTERS

A. Experimental setup

Bimetallic clusters are produced in a dual-target dual-laser vaporization source described in detail elsewhere.[24] Metal vapor is created in the source by the ablation of two rectangular metal targets by means of two pulsed laser beams [7-ns pulses of the second harmonic output of Nd:YAG (yttrium aluminum garnet) lasers]. The condensation chamber has a cylindrical shape, 17 mm long and a diameter of 3 mm; the two vaporization-laser spots are 3 mm apart. The vaporized material is entrained in a short pulse of high purity helium gas introduced by a pulsed supersonic valve. Collisions with the helium gas cool the metal vapor and initiate cluster production. The clusters are further cooled by expansion through a conical nozzle into the vacuum. Charged clusters are accelerated and mass analyzed in a reflectron time-of-flight mass spectrometer ($m/\Delta m \simeq 1000$ around m = 100 amu). For the production of Au_NX_M (X=Sc, Ti, Cr, Fe; N=1–40, M=0–3), the gold target is located at the nozzle side of the source, the transition metal target is placed next to the gas valve.

B. Introducing dopants in gold clusters

Mixed clusters with a wide variety in size and composition can be produced in our source.[10,14,24,25] The abundance of the constituent elements of the bimetallic clusters can be controlled by varying the partial pressures of the two metal vapors and the helium gas. The partial pressures depend on the vaporization laser energies and the time delays of the laser pulses with respect to the gas pulse. These parameters are optimized for each transition metal impurity to obtain for all systems a maximal production of gold clusters containing only a few (one, two or three) dopant atoms. In Table I the applied laser energies, time intervals between the two vaporization laser pulses, and the delay time between introduction of the helium gas and firing the first Nd:YAG laser (vaporizing the dopant material) are listed for the different dopant materials. The helium gas backing pressure is set at 7 bars. The cluster production also is determined by the source geometry, in particular, the distance between the two ablation laser spots, the volume of the condensation chamber, and the diameter and opening angle of the nozzle. For the work presented here we use a conical nozzle, with an opening angle of 10° and a diameter of 1.2 mm at the narrowest point.

TABLE I. Source parameters optimized to obtain a maximal Au_NX^+ signal. E_X and E_{Au} are the applied laser energies in mJ per pulse. The laser spot has a diameter of 1 mm on the target. $\Delta t_{l_1 l_2}$ is the time delay between the firing of the two lasers (dopant material is vaporized as first). Δt_{gl_1} is the time delay between the introduction of the helium gas and the firing of the first laser.

X	E_X (mJ per pulse)	E_{Au} (mJ per pulse)	$\Delta t_{l_1 l_2}$ (μs)	Δt_{gl_1} (μs)
Au		4		590
Sc	22	5	150	480
Ti	25	7	140	490
Cr	23	9	170	470
Fe	22	9	190	430

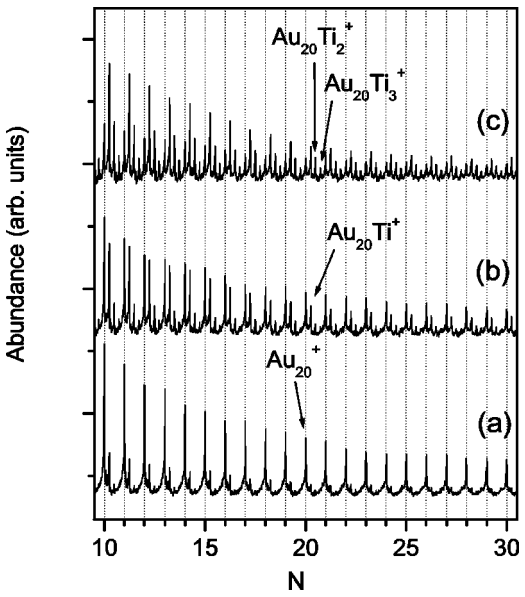

FIG. 1. Abundance spectra of Au_NTi_M bimetallic clusters for different energies of the laser beam vaporizing the titanium target: (a) 20 mJ per pulse, (b) 24.5 mJ per pulse, and (c) 27 mJ per pulse. The laser spot has a diameter of 1 mm on the target.

Probably the most important parameter influencing the production of the bimetallic clusters is the energy density of the laser used for the vaporization of the dopant material. With increasing energy density, a transition occurs from a regime where the production of pure Au_N is barely influenced to a regime with clear signal for gold clusters containing several dopant atoms. Figure 1 displays mass abundance spectra of cationic titanium doped gold clusters for several laser energies of the laser that vaporizes the titanium target, while all other parameters are kept constant. For a laser energy of 20 mJ per pulse only small Au_NTi^+ peaks can be observed. Increasing the energy to 24.5 mJ per pulse enhances the doping, the Au_NTi^+ peaks are almost as high as the pure gold signal, smaller peaks for $Au_NTi_M^+$ (M=2, 3, 4, 5) are visible. A laser energy of 27 mJ per pulse gives rise to a larger signal for singly doped clusters than for pure gold clusters.

III. STABILITY PATTERNS OBTAINED WITH PHOTOFRAGMENTATION SPECTROSCOPY

The stability of $Au_NX_M^+$ (X=Sc, Ti, Cr, Fe; $1 \leqslant N \leqslant 40$, $0 \leqslant M \leqslant 3$) clusters is studied by means of photofragmenta-

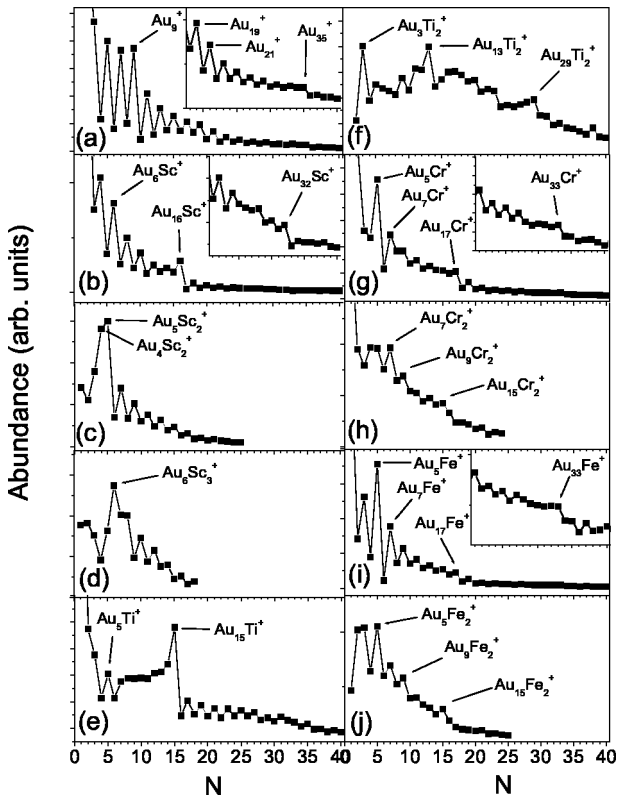

FIG. 2. Measured cationic cluster signals as a function of size for Au_N (a), $Au_N Sc^+$ (b), $Au_N Sc_2^+$ (c), $Au_N Sc_3^+$ (d), $Au_N Ti^+$ (e), $Au_N Ti_2^+$ (f), $Au_N Cr^+$ (g), $Au_N Cr_2^+$ (h), $Au_N Fe^+$ (i), $Au_N Fe_2^+$ (j). Odd-even oscillations and steps in abundance are observed after specific cluster sizes.

tion spectroscopy. In contrast to the mass spectra in Fig. 1, displaying cationic clusters created in the source, the charged particles are now electrostatically deflected out of the beam. The remaining neutral cluster beam is irradiated with high fluence laser light (>2 mJ per pulse, 5-ns pulses, focussed on 1 mm^2) stemming from an ArF excimer laser (photon energy 6.43 eV). Because of the high fluence, each cluster will absorb multiple photons, reach a highly excited and unstable state, and fragment. The formation of stable fragments, which can be as well neutral as charged particles, will be favored during the fragmentation process.[26] The cationic photofragments are recorded with reflectron time-of-flight mass spectrometry. The measured enhanced abundance for certain fragments, compared to the abundance of neighboring masses, will be indicative for their enhanced stability.

The recorded abundances as a function of the cluster size N of photofragmented $Au_N X_M^+$ [$X=$Au, Sc, Ti, Cr, Fe; $M=1,2,(3)$] clusters are shown in Fig. 2. For each measurement at least ten independent mass spectra were averaged and a base line correction was carried out. For multiply doped systems ($M=2,3$) we limited ourself to smaller cluster sizes ($N\leqslant 20$) for which the signals were significantly larger than the noise level and could be well separated from the other (pure and singly doped) cluster peaks.

The abundances do not vary smoothly with increasing cluster size, but one can identify some clear structure. In addition to drops in abundance after specific cluster sizes, the stability patterns reveal distinct odd-even alternations. The strength of the abundance drops and the amplitude of the odd-even alternations strongly depend on both the kind and number of impurities.

A. Au_N^+ ($1\leqslant N\leqslant 40$)

In the photofragmentation spectrum for pure gold clusters a clear odd-even staggering is visible and steps in abundance are recorded after Au_N^+, $N=3$, 9, 19, 21, and 35 [Fig. 2(a)]. These observations can be related with a shell structure and the magic numbers 2, 8, 18, 20, and 34 that arise from the delocalization of the atomic valence $6s$ electrons in the noble metal clusters.[1,27]

B. $Au_N Sc_M^+$ and $Au_N Ti_M^+$ ($1\leqslant N\leqslant 40, M=1,2,3$)

For gold clusters doped with one scandium atom we observe intensity drops at $Au_6 Sc^+$, $Au_{16} Sc^+$, and $Au_{32} Sc^+$ [Fig. 2(b)]. Assuming that each gold atom delocalizes its $6s$ electron as for pure gold clusters, these cluster sizes correspond to 8, 18, and 34 itinerant electrons, provided that the scandium atom delocalizes three electrons.[14] The single titanium doped spectra [Fig. 2(e)] reveal an enhanced stability for $Au_5 Ti^+$ and $Au_{15} Ti^+$. Assuming Ti to delocalize its four valence electrons ($3d^2 4s^2$) these magic clusters contain 8 and 18 itinerant electrons, respectively.[14] The reason that Sc and Ti dopants would delocalize both their $4s$ and $3d$ electrons, is the large spatial extension of d electron wave functions at the beginning of the $3d$ series, which results in a strong hybridization with the Au valence electron orbitals. Remarkable is the strong drop in abundance after $Au_{16} Sc^+$ and $Au_{15} Ti^+$, species corresponding to the magic number 18, while no enhanced stability is recorded for species having 20 delocalized electrons, which is a magic number for pure gold clusters. Such behavior has been attributed to a modification of the effective mean-field potential by the insertion of a dopant atom.[10,11,14]

For multiple scandium and titanium doped gold clusters [Fig. 2(c), 2(d), and 2(f)] we observe an enhanced stability for $Au_4 Sc_2^+$, $Au_5 Sc_2^+$, $Au_6 Sc_3^+$, $Au_3 Ti_2^+$, $Au_{13} Ti_2^+$, and $Au_{29} Ti_2^+$. It is not straightforward to link these observations to electronic shell closure, although the enhanced abundances for the double titanium doped species can be related with the magic numbers 8, 18, and 34 in case the Ti_2 system contributes six electrons to the cloud of itinerant electrons. Following the atomic valence structure of the titanium atom one would expect four (only s) or eight (s and d) delocalized electrons for the dimer. The observation of six electrons contributed by Ti_2 indirectly suggests that the two titanium atoms form a dimer in the gold cluster, and segregation takes place. The experimental observations could be explained by the formation of one localized bond between the two atoms, while the other six valence electrons become itinerant.

The abundance patterns of single, double, and triple scandium doped gold clusters show a clear odd-even staggering. This odd-even staggering is a reflection of an electronic shell structure, since clusters with an even number of delocalized electrons are more stable. For single and triple doped clusters the intensity maxima occur at an even number of gold atoms,

for double doped clusters the intensity maxima correspond with an odd number of gold atoms, indicating that Sc and Sc_3 donate an odd number of electrons and Sc_2 delocalizes an even number of electrons. The odd-even staggering does not show up for the smallest double and triple scandium doped clusters ($N<5$). Remark that, despite the limited information concerning shell closure, the amplitude of the odd-even staggering in the multiple doped spectra is comparable with the one for the single doped spectrum. The fragmentation spectrum for $Au_NTi_2^+$ only reflects odd-even staggering in limited size ranges ($2\leqslant N\leqslant 5$,$8\leqslant N\leqslant 15$, and $18\leqslant N\leqslant 21$).

C. $Au_NCr_M^+$ and $Au_NFe_M^+$ ($1\leqslant N\leqslant 40$,$M=1,2$)

Both for gold clusters doped with a single chromium and a single iron atom, the same magic clusters are found: Au_1X^+, Au_5X^+, Au_7X^+, $Au_{17}X^+$, and $Au_{33}X^+$ ($X=$Cr, Fe). Assuming that two electrons of the dopant atoms are delocalized, these clusters contain 2, 6, 8, 18, and 34 itinerant electrons, respectively.[14] The same magic numbers as for pure gold clusters are obtained if the two dopant valence *s* electrons become itinerant. Note that the atomic valence structure of chromium is $3d^54s^1$ but the promotion energy toward a $3d^44s^2$ configuration is small, which makes it reasonable that this last electron configuration is the preferred one in a gold cluster. Contrary to the Sc and Ti doped clusters, the $3d$ electrons of Cr and Fe remain localized, which agrees with the more contracted *d* orbitals for the heavier $3d$ atoms.

Remarkable are the strongly enhanced abundances for Au_5Cr^+ and Au_5Fe^+, corresponding with six delocalized electrons, while six does not appear as a magic number in pure gold cationic clusters. The enhanced stability for Au_5X^+ species is due to their planar structure (see below) in combination with the 2D magic number six.[23] Note also the disappearance of the magic number 20 (e.g., $Au_{19}X^+$) and the enhancement of the steplike feature corresponding to the magic number 18 (e.g., $Au_{17}X^+$).

For double chromium and iron doped clusters, there is limited information concerning possible shell closures. The only distinguishable drops in abundance occur at $Au_7Cr_2^+$, $Au_9Cr_2^+$, $Au_{15}Cr_2^+$, $Au_5Fe_2^+$, $Au_9Fe_2^+$, and $Au_{15}Fe_2^+$. $Au_7Cr_2^+$ and $Au_5Fe_2^+$ correlate with the magic number eight in case Cr_2 and Fe_2 delocalize respectively two and four electrons in these clusters. It is unclear which shell or subshell closing is related with $Au_9X_2^+$. The steps at $Au_{15}X_2^+$ are smeared out over $N=15,16$ and correspond to the magic number 18 if together the two dopant atoms delocalize four electrons. This is in agreement with the observations for a single dopant, so we cannot make a prediction concerning segregation as for the titanium doped case. The odd-even staggering only is observed for the small sizes ($N<17$) with an amplitude lower than for the singly doped species. Moreover, one can notice some anomalies in the odd-even pattern for the very small clusters ($N=4,5$ for Cr_2 doped and $N=2,3$ for Fe_2 doped gold systems). The pattern for larger sizes suggests that Cr_2 and Fe_2 delocalize an even number of electrons.

D. Summary of the experimental observations

The element and size dependent features observed for the *singly* doped Au_NX^+ clusters are interpreted qualitatively within a simple shell-model approach. From the dopant dependent stability patterns and corresponding magic numbers in photofragmented Au_NX^+ clusters we concluded that the lightest dopants (Sc, Ti) delocalize both their $4s$ and $3d$ electrons, while for the heavier elements (Cr, Fe) only $4s$ electrons are delocalized. This difference is related with the spatial extension of *d* electron wave functions for the different dopants resulting in a stronger (Sc, Ti) or weaker (Cr, Fe) hybridization with the Au valence electron orbitals.[14]

A general trend for all *multiply* doped species is that the electronic shell closures become less pronounced and the amplitude of the odd-even staggering decreases compared to the singly doped clusters. It is not straightforward to count the number of delocalized electrons, nevertheless there is some evidence that Sc_2 and Sc_3 contribute an even and an odd number of electrons, respectively. The titanium dimer would delocalize six electrons, which is not directly related with the atomic valence structure and can indicate segregation in mixed gold-titanium clusters. At least for certain cluster sizes, Cr_2 and Fe_2 behave tetravalent. The disappearance of a clear shell structure compared to the singly doped clusters can have several causes. Possibly the delocalization behavior is size dependent. But more probable, the addition of more transition metal atoms will enhance the *s*-*d* hybridization and increase the importance of localized bonds as in the case of pure transition metal clusters. The raised importance of geometric packing disfavors electronic shell features, which are most pronounced for amorphous simple metal clusters.

IV. CALCULATED PROPERTIES OF Au_5X^+ ($X=$Au, Sc, Ti, Cr, Fe)

A. Calculational level

The aim of this study is to identify in a more quantitative way the dopant dependent differences in the properties of a given cluster structure. Because of the inherently large processing time needed to calculate cluster structures involving heavy atoms (relativistic effects) and transition metals (high spin states possible) at a high level of theory, we have limited this study to AuX^+ dimers and Au_5X^+ clusters ($X=$Au, Sc, Ti, Cr, Fe). The latter systems were chosen because several of the Au_5X^+ clusters appeared to be very stable. The geometries are optimized with DFT using the hybrid B3LYP functional.[28] A relativistic effective core potential with corresponding valence basis set, LANL2DZ,[29] is employed for gold. The Wachters-Hay all electron basis set [6-311+G(d)][30,31] is used for the $3d$ transition metal atoms. The optimization of Au_5X^+ is restricted to triangular structures, having C_{2v} symmetry. Similar structures were calculated as ground-state geometries both for pure $Au_6^{(0,+,-)}$[16,17,34] and zinc doped $Au_5Zn^{(0,+)}$ clusters.[15,22] Vibrational frequency analysis characterized the optimized structures as minima. Charge populations and the occupancy of atomic valence orbitals are obtained with the natural

TABLE II. Cationic dimer bond length (R) and the difference between this bond length and the sum of the atomic radii of the constituent atoms ($\triangle R$). The AuX^+ and Au_5X^+ atomization energies (D_e) as defined in Eqs. (1) and (2). The last column contains the highest occupied molecular orbital (HOMO) lowest unoccupied molecular orbital (LUMO) gap ($E_{H\text{-}L}$) of the Au_5X^+ species.

X	R (Å) AuX^+	$\triangle R$ (Å) AuX^+	D_e (eV) AuX^+	D_e (eV) Au_5X^+	$E_{H\text{-}L}$ (eV) Au_5X^+
Au	2.705	−0.18	1.87	9.99	1.06
Sc	2.469	−0.58	3.49	12.12	1.40
Ti	2.428	−0.46	2.98	11.35	2.52
Cr	2.435	−0.26	1.24	9.68	2.44
Fe	2.359	−0.32	2.43	9.41	2.18

population analysis (NPA).[32] All calculations are performed with the GAUSSIAN 98 package.[33]

B. Geometry, charge transfer, and stability

The calculated cationic dimer bond lengths are given in Table II together with the contraction compared to the sum of the atomic radii of gold and the impurity atom. The magnitude of contraction is reasonable for all dopants. $\triangle R$ is larger for $AuSc^+$ and $AuTi^+$ than for the $AuCr^+$ and $AuFe^+$ dimers. A similar dopant dependent trend was observed for transition metal doped Cu_{12} and Ag_{12} clusters.[7,8]

Optimization of Au_5X^+ (X=Au, Sc, Ti, Cr, Fe) started from the triangular ground-state structure of Au_5Zn^+,[15,22] in which the zinc atom is replaced by the respective dopant atom. In all cases a stable triangular isomer that resembles the initial structure was found, as shown in Fig. 3. The calculated Au_6^+ cluster is only slightly distorted from D_{3h} symmetry, and corresponds very well to the ground-state structures for $Au_6^{(0,+,-)}$ found in literature.[16,17,34] The Au-X bond lengths in the Au_5X^+ (X=Ti, Cr, Fe) structures are shorter than the corresponding Au-Au bonds in Au_6^+, due to the smaller radius of the dopant atoms (see Table II). A more drastic change occurs when the cluster is doped with a scandium atom. The structure of Au_5Sc^+ differs from the other Au_5X^+ systems, the scandium atom is shifted much more

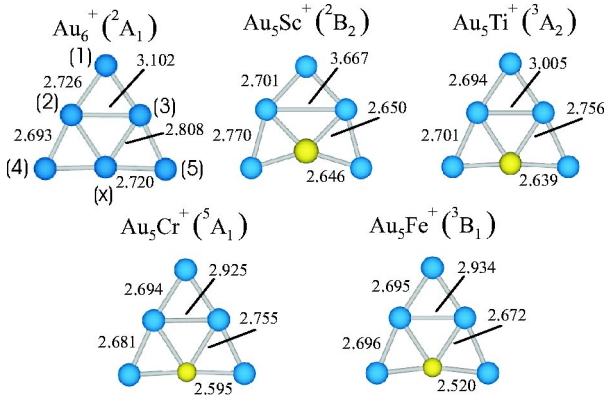

FIG. 3. (Color online) Optimized structures for Au_5X^+ (X=Au, Sc, Ti, Cr, Fe). Bond lengths are given in angstrom.

TABLE III. Charge on the different atoms in AuX^+ and Au_5X^+ obtained with NPA. The gold atoms are numbered as presented for Au_6^+ in Fig. 3. $\triangle EN$ is the difference in electronegativity of Au and X according to the Pauling scale.

X	$\triangle EN$	Charge (a.u.) AuX^+ X	Charge Au_5X^+ (a.u.) X	Au(1)	Au(2), Au(3)	Au(4), Au(5)
Au	0.0	+0.50	+0.24	+0.25	+0.12	+0.14
Sc	1.1	+1.22	+0.89	+0.10	+0.07	−0.07
Ti	0.9	+1.19	+0.84	+0.11	+0.10	−0.08
Cr	0.8	+1.05	+0.84	+0.13	+0.09	−0.07
Fe	0.6	+0.93	+0.76	+0.12	+0.10	−0.04

towards the center of the cluster. The bond distances between Sc and the neighboring Au atoms are shorter than those in Au_6^+, despite the large size of the Sc atom. However the insertion of the Sc atom causes a significant elongation of the Au(2)-Au(3) [and Au(2)-Au(4)] bond distance (the gold atom numbering is defined for Au_6^+ in Fig. 3). The energetic disadvantage of the stretched Au-Au bond is compensated by stronger Au-Sc bonds. The highest occupied molecular orbital (HOMO) of Au_5Sc^+ (see Fig. 5) is bonding between Sc and the four neighboring gold atoms, but antibonding between Au(2) and Au(3) as well as between Au(2) and Au(4), and leads to stronger Au-Sc bonds and longer Au-Au distances. A similar molecular orbital is not occupied for the other Au_5X^+ species as will be discussed in Sec. IV C.

Charge populations obtained with NPA are given in Table III. The transition metal dopants lose almost an entire electron charge to make the cluster cationic. The absolute value of the positive charge on the dopant atom correlates with the difference in electronegativity between X and Au. Note that the schemes to assign charges are to some extent arbitrary because atomic charge is not a quantum-mechanical observable. The charges of the dopant atom obtained with Mulliken charge population analysis were higher than the ones obtained with NPA. The positive charge is on the dopant atom because this atom has the lowest electronegativity. The larger electron transfer leads to partial ionic and therefore stronger bonds, which gives rise to enhanced atomization energies. The atomization energies are calculated as follows:

$$D_e(AuX^+) = E_{Au} + E_{X^+} - E_{AuX^+}, \quad (1)$$

$$D_e(Au_5X^+) = 5E_{Au} + E_{X^+} - E_{Au_5X^+}, \quad (2)$$

where E_M is the total energy of M. The atomization energies for both AuX^+ and Au_5X^+ are presented in Table II. Doping with scandium and titanium enhances the stability of the cluster compared with pure gold, correlating with the large bond length contraction, while doping with chromium and iron slightly reduces the stability. One should note that this result is only valid for the studied triangular isomers of Au_5X^+, which not necessarily are the ground-state structures. Nevertheless, there is a correspondence between the calculated atomization energies and the measured Au_NX^+

cluster abundances: we recorded larger absolute signals for scandium and titanium doped than for chromium and iron doped gold clusters.

C. Density of states and molecular-orbital patterns

In this section we focus on the electronic structure of the clusters presented in Fig. 3. Both the density of states and the shape of some specific molecular orbitals are considered. The density of states (DOS) was obtained from the discrete energy levels using a Lorentz expansion scheme

$$\mathrm{DOS}(E) = \sum \frac{\delta/\pi}{(E-\varepsilon_i)^2+\delta^2}, \tag{3}$$

where the sum is made over all occupied levels (ε_i): spin-up and spin-down states are considered separately, a broadening factor $\delta = 0.20$ eV is used. The DOS is shifted in energy to place the Fermi level at zero (shift of 11.01 eV for Au_6^+, 9.63 eV for Au_5Cr^+, 10.07 eV for Au_5Ti^+, 11.13 eV for Au_5Cr^+, and 11.17 eV for Au_5Fe^+). The result is given in Fig. 4, the spin-down density is plotted as negative. The HOMO level (at zero energy) is indicated by the dashed line, the lowest unoccupied molecular orbital (LUMO) level by a dotted line. The energy of the HOMO-LUMO gap is given in Table II. A large HOMO-LUMO gap is obtained for Au_5Ti^+, Au_5Cr^+, and Au_5Fe^+. According to the shell-model interpretation described earlier, the number of delocalized electrons in these clusters is eight, six, and six, respectively. Where six is a magic number for planar clusters, eight is a magic number both for triangular planar and for spherical clusters.[23,1,2] On the other hand, for Au_6^+ and Au_5Sc^+ we predicted an odd number of delocalized electrons; this nonstabilized electronic state agrees with the calculated smaller HOMO-LUMO gap.

All studied species have an intense 'band' in the DOS between 0 eV and -5 eV, which is composed mainly of the valence *s* and *d* orbitals of the constituent atoms. The *s* and *d* electrons are strongly hybridized. This is related with the relativistic contraction of the atomic Au 6*s* orbitals, which leads to a shortening of the interatomic bond distances and an increased *s*-*d* and *d*-*d* overlap for electrons stemming from neighboring atoms. The imbalance between spin-up and spin-down states is a reflection of the local magnetic moment, which is especially large in the case of the chromium doped cluster.

One can distinguish two types of orbitals for the studied bimetallic clusters. Most molecular orbitals are ''localized.'' They are build up mainly from *d* electrons that are localized on one specific atom and there only is a negligible overlap between the different parts of the wave function. Some molecular orbitals have a more delocalized character. They are build up mainly from *s* electrons, and 3*d* electrons in the case of scandium and titanium, and spread out over the entire cluster. We will link these orbitals to the itinerant electrons in the shell model. This way a comparison can be made between the high-level DFT calculations and the phenomenological shell-model interpretations. The energies of the delocalized orbitals are indicated in Fig. 4 by the arrows and their

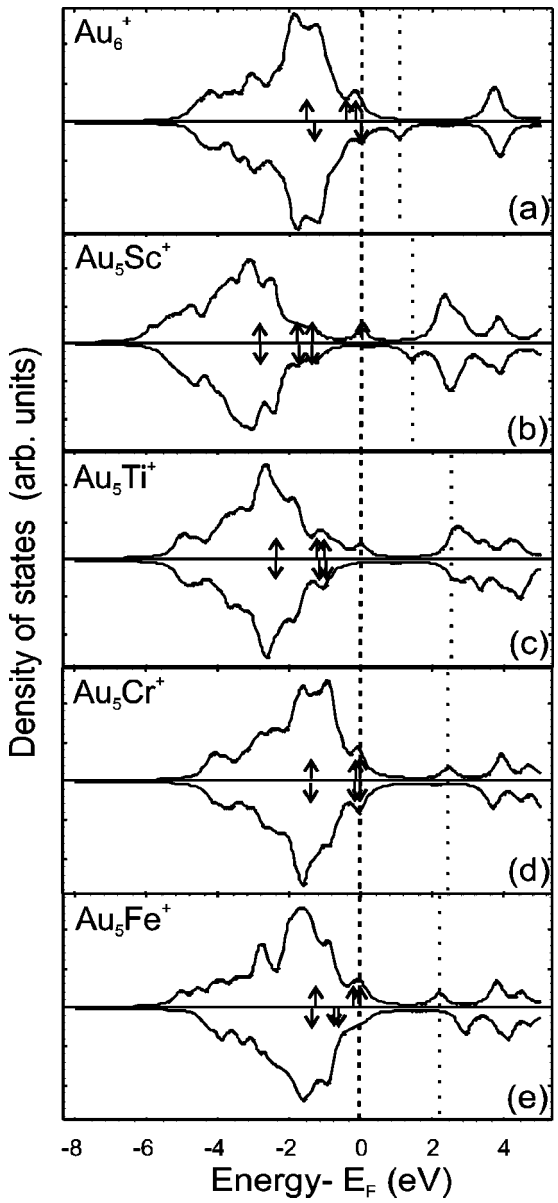

FIG. 4. Density of states for the structures shown in Fig. 3. (a) Au_6^+, (b) Au_5Sc^+, (c) Au_5Ti^+, (d) Au_5Cr^+, (e) Au_5Fe^+. Spin up (positive) and spin-down (negative) densities are given in each case. The arrows are placed at energies corresponding with the delocalized molecular orbitals. The entire spectra are energetically shifted as such that zero energy corresponds with the HOMO (given by the dashed line). The dotted lines locate the LUMO.

electron density is plotted in Fig. 5. The valence-electron occupancy of the dopant atom (*X*) is listed in Table IV.

The delocalized molecular orbitals for all studied systems are alike. The lowest delocalized orbital, in energy between the localized MO's built up from atomic *d* orbitals, has no nodal planes (*s* wave function). The next two levels have one nodal plane perpendicular to the molecular frame (p_x and p_y wave functions). These levels are the HOMO and HOMO-1 levels in all cases except for the scandium and titanium doped systems. The *s* and *p* molecular orbitals are shaped alike the three lowest energetic wave functions pos-

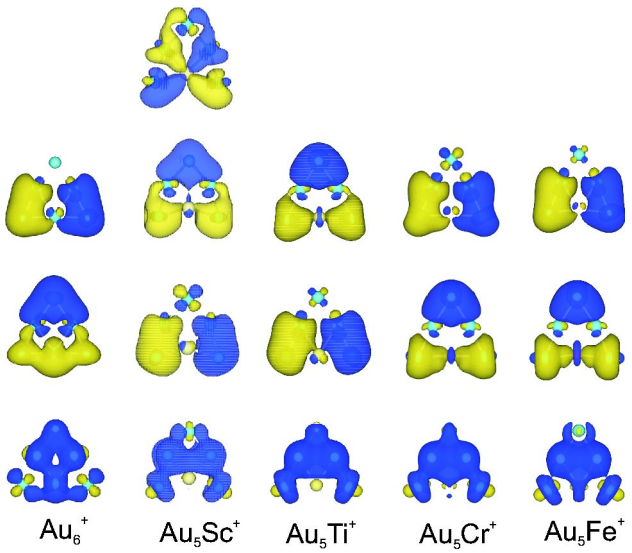

FIG. 5. (Color online) Plot of the molecular orbitals that are delocalized over the entire cluster. The energy of the orbitals is indicated with the arrows in Fig. 4, the lowest energy states are below. All shown orbitals are doubly occupied, except the energetic highest orbitals of Au_6^+ and Au_5Sc^+. This means that the number of delocalized electrons in these clusters are: five for Au_6^+, seven for Au_5Sc^+, and six for Au_5Ti^+, Au_5Cr^+, and Au_5Fe^+.

sible for a particle in a two-dimensional box. Filling these levels will add up to six itinerant electrons, being a magic number for planar shaped structures.[23] In the case of Au_5Sc^+ there is an extra delocalized level with a d_{xy} shape. All shown molecular orbitals are doubly occupied except for the energetic highest orbitals for Au_6^+ and Au_5Sc^+. This means that the number of itinerant electrons in these clusters is: five for Au_6^+, seven for Au_5Sc^+, six for Au_5Ti^+, six for Au_5Cr^+, and six for Au_5Fe^+. This is the same conclusion we reached when interpreting the photofragmentation spectra on the basis of a phenomenological shell model, except for Au_5Ti^+ where eight itinerant electrons were assigned. We will discuss this last point in more detail in Sec. V.

D. Local magnetic moments

Not only the structural and electronic properties of the clusters are dopant dependent, also their magnetic behavior will be different. In this paragraph we examine the influence of the surrounding gold atoms on the local magnetic moment of the impurity. Open shell atoms are magnetic in their ground state according to Hund's rules. If atoms bind, some discrete localized atomic orbitals can delocalize or hybridize, the atomic levels disperse in energy and can give rise to energy bands. Magnetism is quenched in many bulk systems because of this delocalization. Extensive studies on the behavior of $3d$ ions in different kinds of bulk metals, surfaces, and clusters have been performed.[35,36] In all cases, the local magnetism was sensitive to the local structure and environment. In small clusters, the coordination of the dopant is limited, $3d$ electrons remain reasonably localized.

TABLE IV. Valence-electron occupancy (Occ.) of the dopant atom (X) as: free atom, cation, in AuX^+ and in Au_5X^+. No difference is made between different spin states. The occupancy of Rydberg states (mainly $4p$ or $6p$) is also given, in this number also higher contributions (which all are very small) are included.

X	Occ. X	Occ. X^+	Occ. AuX^+	Occ. Au_5X^+
Au	$6s^1 5d^{10}$	$6s^0 5d^{10}$	$6s^{.55} 5d^{9.93} 6p^{.02}$	$6s^{.87} 5d^{9.81} 6p^{.01}$
Sc	$4s^2 3d^1$	$4s^1 3d^1$	$4s^{.65} 3d^{1.10} 4p^{.03}$	$4s^{.59} 3d^{1.40} 4p^{.12}$
Ti	$4s^2 3d^2$	$4s^{0.7} 3d^{2.3}$	$4s^{.44} 3d^{2.34} 4p^{.03}$	$4s^{.51} 3d^{2.48} 4p^{.16}$
Cr	$4s^1 3d^5$	$4s^0 3d^5$	$4s^{.44} 3d^{4.48} 4p^{.03}$	$4s^{.55} 3d^{4.49} 4p^{.11}$
Fe	$4s^2 3d^6$	$4s^0 3d^7$	$4s^{.78} 3d^{6.25} 4p^{.04}$	$4s^{.72} 3d^{6.39} 4p^{.12}$

The magnetic moment is related to the spin imbalance through the g factor, which we assumed to be equal to the free-electron value. As such the magnetic moment is the difference between occupation numbers in spin-up and spin-down states. NPA is used to obtain the occupation numbers of the atomic orbitals for different spin states. The local magnetic moment on the dopant atom and the averaged magnetic moment of the five gold atoms in Au_5X^+ are given in Table V and compared with the magnetic moments of the free atom, free ion and of X in the cationic dimer. One can note that the dopant atoms having a large magnetic moment as free atom or ion, still have a large magnetic moment in Au_5X^+, although it is reduced (except for titanium). The reduction is considerable for iron and scandium dopants, and smaller for doping with chromium.

Previous studies have shown that charge transfer and hybridization of valence electrons stemming from host and impurity importantly influence the local magnetic moment.[7,37] In general, the magnetic moment of the impurity decreases with an increasing amount of neighboring atoms. The local magnetic moment of the scandium doped system is quenched because of the strong d-d hybridization due to the spatially extended scandium d orbitals. For larger dopants (Cr, Fe) d-d hybridization is less important, there is almost no d orbital overlap because the d orbitals of the heavier transition metals are more contracted. The main influence on occupancy of the impurity d orbitals arises from s-d and p-d interactions.

TABLE V. Local magnetic moments (in μ_B) of the dopant atom: as free atom, free ion, in AuX^+ and in Au_5X^+. The last column lists the averaged magnetic moment on the gold atoms in Au_5X^+.

X	μ_X	μ_{X^+}	μ_X AuX^+	μ_X Au_5X^+	$\mu_{\mathrm{Au,avg}}$ Au_5X^+
Au	1	0	0.50	0.30	0.14
Sc	1	2	1.02	0.36	0.13
Ti	2	1	2.05	1.93	0.01
Cr	6	5	4.19	4.17	−0.03
Fe	4	3	3.91	1.85	0.03

V. 2D VERSUS 3D STRUCTURES

In this section we focus on the dimensionality of the studied clusters. Stable planar triangular isomers were found for the studied Au_5X^+ systems. This is in line with previous theoretical and experimental work on pure gold clusters, where evidence was found for planar ground-state structures up to fairly large sizes (up to $N=7$ for neutrals and cations, and up to $N=12$ for anions).[16,17,18] The preference for planar isomers is related to the large mass of the gold atoms. Relativistic effects lower the energy and shrink the size of the 6s orbital, allowing a larger degree of $6s$-$5d$ hybridization and therefore stronger and more directional bonds. The overlap of the $5d$ orbitals is optimal for a planar configuration. Systems composed of lighter atoms already become 3D for smaller sizes [e.g., Ag_5^+ (Ref. 38) and Li_6 (Ref. 39) are 3D].

As shown above, introducing a dopant can drastically change cluster properties such as electronic structure, dissociation energy, magnetic moment, or size dependent stability. Here we will address the question whether one can construct a three-dimensional cluster just by replacing one atom in a planar cluster.

In our recent work on $Au_NZn^{(0,+)}$ ($N\leqslant 6$) all ground-state structures were computed to be 2D.[15] As for pure clusters[40] strong s-d hybridization was found to have a major influence on the planarity of the Au_NZn systems. Additionally, the dopant Zn atom promotes the 2D isomers through extra σ bonding formed by overlap between vacant $4p$ orbitals of Zn and the atomic valence $6s$ and $5d$ orbitals of Au. Similar phenomena occur in the Au_5X^+ systems studied in this work, also favoring the 2D isomers.

The photofragmentation experiments for Au_NTi^+ suggested that as well the s as the d electrons of titanium are delocalized over the cluster volume, meaning that the Au_5Ti^+ cluster has eight delocalized electrons. On the other hand, the calculated MO pattern for the planar triangular Au_5Ti^+ isomer showed only three filled delocalized orbitals (six electrons), the other electrons occupied localized molecular orbitals consisting of atomic d orbitals. For the other Au_5X^+ ($X=$Au, Sc, Cr, Fe), the experimentally determined number of itinerant electrons agreed with the molecular orbital pattern.

Eight is a magic number for 3D clusters. Optimization of 3D isomers for Au_5Ti^+ lead to a trigonal bipyramid arrangement (C_{2v}) in which the titanium atom is fivefold coordinated as shown in Fig. 6. This isomer is only 0.41 eV higher in energy than the planar triangular isomer, despite the limited number of Au-Au bonds. This is in contrast with Au_5Zn^+ for which, notwithstanding the exhaustive search, no 3D isomer was found.[15] The 3D isomer of Au_5Ti^+ has four doubly occupied delocalized orbitals (singlet state), or eight itinerant electrons in agreement with the 3D magic number. In case of the 2D triangular isomer the third p shaped molecular orbital, having a node in the molecular plane, was energetically unfavorable and for that reason unoccupied.

To link this result with the experimental observation, two situations are possible. Or Au_5Ti^+ is planar and has six delocalized electrons, meaning that the number of delocalized electrons is size dependent ($Au_{15}Ti^+$ corresponds with the magic number 18). Or the cluster is 3D and has eight delocalized electrons.

One can conclude, that there is a strong correlation between the shape of the cluster, leading to certain magic numbers and the number of delocalized electrons.

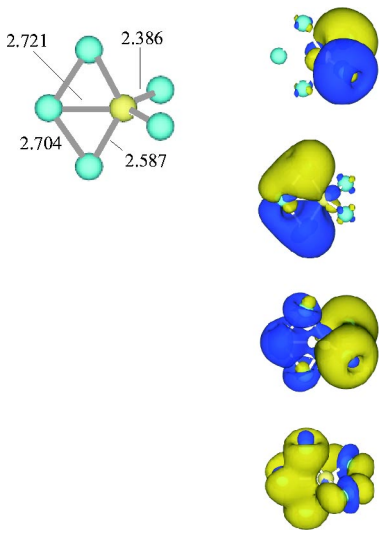

FIG. 6. (Color online) On the left-hand side the optimized 3D structure for Au_5Ti^+ (C_{2v}, $^1A_1$) is presented. Bond lengths are given in angstrom. On the right-hand side the delocalized molecular orbitals are plotted. All shown orbitals are doubly occupied; there are in total eight delocalized electrons in this isomer.

VI. CONCLUSIONS

In this work Au_NX_M clusters ($X=$Sc, Ti, Cr, Fe; $N=1$–40, $M=0$–3) were studied. Stability patterns obtained in photofragmentation experiments revealed a shell structure in the singly transition metal doped gold species. The number of itinerant electrons arising from the dopant depends on the extension of their atomic d orbitals. For higher doped systems the electronic shell structure is less clear. Probably interactions involving the relatively large transition metal d electron orbitals lead to the formation of more localized bonds, like in pure transition metal clusters.

DFT studies on the Au_5X^+ species showed that depending on the dopant the stability of the gold cluster can be enhanced or reduced. From the dopant point of view, their local magnetic moment is not screened completely by interaction with the surrounding gold atoms. All studied species had some delocalized molecular orbitals. The number of electrons in these orbitals corresponds with the number of delocalized electrons we deduced from the interpretation of the experiments, based on a phenomenological shell model. For the Au_5Ti^+ system it was shown that the number of delocalized electrons not only depends on the number and kind of the constituent atoms but also on the shape of the cluster.

ACKNOWLEDGMENTS

This work is financially supported by the Fund for Scientific Research—Flanders (Belgium) (FWO), the Flemish Concerted Action (GOA) Research Program, and the Interuniversity Poles of Attraction Program (IAP)—Belgian State, Prime Minister's Office—Federal Office for Scientific, Technical and Cultural Affairs. E.J. and S.N. thank the FWO for financial support.

*Present address: Laboratory for Organometallic Photodynamics, Photodynamics Research Center, RIKEN, Sendai, Miyagi 980-0845, Japan.

†Electronic address: Peter.Lievens@fys.kuleuven.ac.be

[1] W.A. de Heer, Rev. Mod. Phys. **65**, 611 (1993).
[2] K. Clemenger, Phys. Rev. B **32**, 1359 (1985).
[3] T.P. Martin, Phys. Rep. **273**, 199 (1996).
[4] I.M.L. Billas, A. Châtelain, and W.A. de Heer, Science **265**, 1682 (1994).
[5] G. Ganteför and W. Eberhardt, Phys. Rev. Lett. **76**, 4975 (1996).
[6] Y. Yamada and A.W. Castleman, Jr., J. Chem. Phys. **97**, 4543 (1992).
[7] Q. Sun, X.G. Gong, Q.Q. Zheng, D.Y. Sun, and G.H. Wang, Phys. Rev. B **54**, 10 896 (1996).
[8] Q. Sun, Q. Wang, J.Z. Yu, Z.Q. Li, J.T. Wang, and Y. Kawazoe, J. Phys. I **7**, 1233 (1997).
[9] J. Van De Walle, R.J. Tarento, and P. Joyes, Surf. Rev. Lett. **6**, 307 (1999).
[10] W. Bouwen, F. Vanhoutte, F. Despa, S. Bouckaert, S. Neukermans, L.T. Kuhn, H. Weidele, P. Lievens, and R.E. Silverans, Chem. Phys. Lett. **314**, 227 (1999).
[11] M. Heinebrodt, N. Malinowski, F. Tast, W. Branz, I.M.L. Billas, and T.P. Martin, J. Chem. Phys. **110**, 9915 (1999).
[12] K. Koyasu, M. Mitsui, A. Nakajima, and K. Kaya, Chem. Phys. Lett. **358**, 224 (2002).
[13] X. Li, B. Kiran, J. Li, H.J. Zhai, and L.S. Wang, Angew. Chem. **114**, 4980 (2002).
[14] S. Neukermans, E. Janssens, H. Tanaka, R.E. Silverans, and P. Lievens, Phys. Rev. Lett. **90**, 033401 (2003).
[15] H. Tanaka, S. Neukermans, E. Janssens, R. E. Silverans, and P. Lievens, J. Chem. Phys. **119**, 7115 (2003).
[16] H. Häkkinen and U. Landman, Phys. Rev. B **62**, R2287 (2000).
[17] S. Gilb, P. Weis, F. Furche, R. Ahlrichs, and M.M. Kappes, J. Chem. Phys. **116**, 4094 (2002).
[18] V. Bonačić-Koutecký, J. Burda, R. Mitrić, M. F. Ge, G. Zampella, and P. Fantucci, J. Chem. Phys. **117**, 3120 (2002).
[19] P.A. Christiansen, W.C. Ermler, and K.S. Pitzer, Annu. Rev. Phys. Chem. **36**, 407 (1985).
[20] U. Landman, W.D. Luedtke, N.A. Burnham, and R.J. Colton, Science **248**, 454 (1990).
[21] H. Häkkinen and U. Landman, J. Am. Chem. Soc. **123**, 9704 (2001).
[22] H. Tanaka, S. Neukermans, E. Janssens, R.E. Silverans, and P. Lievens, J. Am. Chem. Soc. **125**, 2862 (2003).
[23] E. Janssens, H. Tanaka, S. Neukermans, R.E. Silverans, and P. Lievens, New J. Phys. **5**, 46 (2003).
[24] W. Bouwen, P. Thoen, F. Vanhoutte, S. Bouckaert, F. Despa, H. Weidele, R.E. Silverans, and P. Lievens, Rev. Sci. Instrum. **71**, 54 (2000).
[25] P. Lievens, P. Thoen, S. Bouckaert, W. Bouwen, F. Vanhoutte, H. Weidele, and R.E. Silverans, Chem. Phys. Lett. **302**, 571 (1999).
[26] C.E. Klots, J. Phys. Chem. **92**, 5864 (1988).
[27] I. Katakuse, T. Ichihara, Y. Fujita, T. Matsuo, T. Sakurai, and H. Matsuda, Int. J. Mass Spectrom. Ion Processes **67**, 229 (1985).
[28] A.D. Becke, J. Chem. Phys. **98**, 5648 (1993).
[29] P.J. Hay, W.R. Wadt, J. Chem. Phys. **82**, 299 (1985).
[30] A.J.H. Wachters, J. Chem. Phys. **52**, 1033 (1970).
[31] P.J. Hay, J. Chem. Phys. **66**, 4377 (1977).
[32] A.E. Reed, R.B. Weinstock, and F. Weinhold, J. Chem. Phys. **83**, 735 (1985).
[33] M. J. Frisch *et al.*, Computer code GAUSSIAN 98, Revision A.7 (Gaussian, Inc., Pittsburg PA, 1998).
[34] G. Bravo-Pérez, I.L. Garzón, and O. Novaro, Chem. Phys. Lett. **313**, 655 (1999).
[35] D. Riegel, L. Büermann, K.D. Gross, M. Luszik-Bhadra, and S.N. Mishra, Phys. Rev. Lett. **62**, 316 (1989).
[36] P. Blaha and J. Callaway, Phys. Rev. B **33**, 1706 (1986).
[37] X.S. Chen, J.J. Zhao, and G.H. Wang, Z. Phys. D: At., Mol. Clusters **35**, 149 (1995).
[38] P. Weis, T. Bierweiler, S. Gilb, and M.M. Kappes, Chem. Phys. Lett. **355**, 355 (2002).
[39] I. Boustani, W. Pewestorf, P. Fantucci, V. Bonačić-Koutecký, and J. Koutecký, Phys. Rev. B **35**, 9437 (1987).
[40] H. Häkkinen, M. Moseler, and U. Landman, Phys. Rev. Lett. **89**, 033401 (2002).